

A Signature Based Approach Towards Global Channel Charting with Ultra Low Complexity

Longhai Zhao, Yunchuan Yang, Qi Xiong, He Wang, Bin Yu, Feifei Sun, and Chengjun Sun
Advanced Research & Standard Team, Samsung Research Institute China – Beijing (SRC-B), Beijing, P. R. China
{longhai.zhao, yc0301.yang, q1005.xiong, h0809.wang, bin82.yu, feifei.sun, chengjun.sun}@samsung.com

Abstract—Channel charting, an unsupervised learning method that learns a low-dimensional representation from channel information to preserve geometrical property of physical space of user equipments (UEs), has drawn many attentions from both academic and industrial communities, because it can facilitate many downstream tasks, such as indoor localization, UE handover, beam management, and so on. However, many previous works mainly focus on charting that only preserves local geometry and use raw channel information to learn the chart, which do not consider the global geometry and are often computationally intensive and very time-consuming. Therefore, in this paper, a novel signature based approach for global channel charting with ultra low complexity is proposed. By using an iterated-integral based method called signature transform, a compact feature map and a novel distance metric are proposed, which enable channel charting with ultra low complexity and preserving both local and global geometry. We demonstrate the efficacy of our method using synthetic and open-source real-field datasets.

Index Terms—channel charting, indoor localization, signature transform, unsupervised learning, dimensionality reduction

I. INTRODUCTION

Channel charting (CC) is an unsupervised learning method that uses channel information (CI) to extract a low-dimensional embedding (i.e., the chart) that preserves geometrical structure of physical space of user equipments (UEs), which facilitates a broad distance-based or location-based applications, such as handover [1], indoor localization [2], beam management [4], pilot management [5], and so on. Thus, CC is an attractive and promising approach to enable many applications in beyond 5G and 6G systems. Roughly speaking, CC most often consists of three main steps: 1.) construct a suitable feature map of the CI, 2.) design a distance metric for the CI or feature map in such a way that the distance between two feature maps is proportional to the physical distance between the corresponding UEs, 3.) use a dimensionality reduction method to obtain the chart.¹

However, in CC studies so far, the raw channel information, e.g., channel impulse response (CIR) or channel frequency response (CFR), and their simple variants are still commonly used as feature maps to learn the chart. For instance, channel features in angular domain are proposed for CC in [1] [11], which do not apply for scenarios with single-antenna base stations (BSs). The magnitude of CIR is used as feature map in [2] and the magnitude of truncated CIR is used in [3]. All existing feature maps used for CC are still very

high-dimensional owing to the increasing sampling rate in the spatial, frequency, and time domains, which increase the complexity of subsequent procedures for CC, e.g., the pairwise distance calculation, the operations for training and inference of neural networks. Since CC is a similarity/dissimilarity learning based method and the number of pairwise distance is proportional to the squared number of training samples, more training time is needed for neural network based CC. Therefore, a compact and suitable feature map is very appealing for practical implementations of CC. But there is still a lack of systematic ways for deriving a feature map that is low-dimensional, sampling-rate-agnostic and suitable for CC.

When using parametric approaches, such as Siamese network or triplet network, to learn the chart, designing a faithful distance metric is crucial for a successful CC. However, the UE trajectory or distribution in real environments often exhibits a geometrical structure that is locally linear and globally nonlinear, which poses challenges to design a simple metric that is faithful for both local and global geometry. Using the norm of channel features in angular domain [1], time domain [2], or timestamps of consecutive CI [11] as a metric only preserves the local geometry, which makes the resulting CC inappropriate for tasks like indoor localization. In order to obtain a distance metric that is suitable for both local and global geometry, the CIR geodesic distance is proposed in [2]. However, to generate the pairwise CIR geodesic distance matrix, one needs to specify a suitable neighborhood number, which is a non-trivial task and dependent on particular UE trajectories or distributions. In addition, constructing the neighborhood graph and calculating the geodesic distance are also computationally intensive.

Therefore, to address these issues in the first two steps of CC, a signature based approach that generates a global chart with ultra low complexity is proposed in this paper. Instead of using truncation [3] or downsampling [11] to reduce the number of channel features, we take a totally opposite way, in which the dimensionality of raw discrete CIRs is firstly lifted to form continuous functions and then reduced significantly to obtain a compact feature map by using signature transform, an iterated-integrals based transformation. The signature transform is a nonlinear mapping from a path (continuous mapping) to an infinite sequence called signature, which was originally introduced by [6] and has been used in finance [9], rough path theory [7], machine learning [8], and so on. The signature

¹For some non-parametric approaches, such as principal component analysis, no need to specify a distance metric explicitly.

provides a well summary of the path and has meaningful interpretations from the geometrical or statistical viewpoint. With the proposed feature map, a signature based principal component analysis (SPCA) is proposed for CC, in which the dimensionality of the covariance matrix is very small and only proportional to the number of BSs. For parametric approaches, we propose a signature based Siamese network (SSN) for CC. In order to train the network efficiently in terms of both performance and complexity, a novel distance metric that is valid for both local and global geometry is also proposed, without calculating geodesic distance or constructing neighborhood graph. We evaluate the proposed methods on a synthetic dataset and two open-source real-field datasets.

The outline of the paper is as follows. The preliminaries of path signature are introduced in Section II. Then, the proposed signature-based approach is presented in Section III with the introduction of feature map derivation, SPCA and SSN based CC. Eventually, the experimental results are given and demonstrate the superiority of the proposed approach.

II. PRELIMINARIES OF PATH SIGNATURE

A d -dimensional path (parameterized by τ) is a continuous mapping from a real interval $[a, b]$ to \mathbb{R}^d , and can be denoted as $X(\tau) = \{X_1(\tau), \dots, X_d(\tau)\} : [a, b] \rightarrow \mathbb{R}^d$. The signature of $X(\tau)$ is defined as the collection of iterated integrals, i.e.,

$$\mathbf{S}(X) = (1, S(X)_1, \dots, S(X)_d, \dots, S(X)_{i_1, i_2, \dots, i_k}, \dots) \quad (1)$$

where "1" as the first term of $\mathbf{S}(X)$ denotes the 0-th level signature, and $S(X)_{i_1, i_2, \dots, i_k}$ denotes one of the k -th level (k is an integer and $k \geq 1$) signature features and given by [8]

$$S(X)_{i_1, i_2, \dots, i_k} = \int_a^{\tau_1} \dots \int_{\tau_{k-1}}^{\tau_k} dX_{i_1}(\tau_1) \dots dX_{i_k}(\tau_k) \quad (2)$$

where $i_k \in \{1, 2, \dots, d\}$, and the integral can be understood as Riemann integral with $dX_{i_k}(\tau_k) = \frac{dX_{i_k}}{d\tau}(\tau_k)d\tau_k$ when the underlying path is differentiable.

Due to the nature of integral, each signature feature can be interpreted as a geometrical item like length, area, volume, and so on. Moreover, each signature feature can also be viewed as a statistical feature. For example, let τ be a random variable following uniform distribution over $[a, b]$, then the first and second level signature features are given by

$$S(X)_i = \int_a^b dX_i(\tau) \propto \mathbb{E}_\tau[\dot{X}_i(\tau)] \quad (3)$$

$$S(X)_{i,j} = \int_a^b \int_a^b dX_i(\tau_1) dX_j(\tau_2) \propto \mathbb{E}_{\tau_1 < \tau_2}[\dot{X}_i(\tau_1) \dot{X}_j(\tau_2)] \quad (4)$$

where $\dot{X}_i(\tau) = \frac{dX_i(\tau)}{d\tau}$, $i, j \in \{1, 2, \dots, d\}$. Thus, $S(X)_i$ measures the averaged change of random variable X_i over the interval $[a, b]$. $S(X)_{i,j}$ measures the covariance of changes between X_i and X_j at two ordered points, which makes it different from ordinary statistics like moments that do not have any ordering constraints.

The signature has some nice properties that make it very suitable for CC. For example, the mapping from the path to its signature is continuous, injective under a mild condition, and the signature can approximate the path arbitrarily well by linear combination [8]. Most importantly, the ability to preserve the ordering information for sequential data makes the signature very suitable for distance-based learning algorithms.

It is also worth to note that the features of signature are not independent from each other. To eliminate the redundant information of the signature, a more compact form can be obtained by its logarithm, which is defined as [6]

$$\log(\mathbf{S}) \triangleq \sum_{m=1}^{\infty} \frac{(-1)^{(m-1)}}{m} (\mathbf{S} - \mathbf{1})^{\otimes m} \quad (5)$$

where $\mathbf{1} = (1, 0, 0, \dots)$, and \otimes denotes the tensor product over non-commutative tensor algebra [7]. For the remainder of this paper, we will refer to the feature obtained by (5) as the signature. Moreover, a truncation of the signature is usually applied for practical usage.

III. THE PROPOSED SIGNATURE BASED CC

Consider a single-input single-output (SISO) communication system in which UEs communicate to N_b BSs.² We have a dataset with D samples of raw CIRs for all links between BSs and any UE, which can be denoted as a set of matrices $\{\mathbf{H}_i\}$ with \mathbf{H}_i being a $N_b \times 2N$ real matrix, $i \in \mathcal{D} := \{1, 2, \dots, D\}$ is the sample index and N is the number of taps.³ With this dataset, the objective of CC is to learn a low-dimensional embedding, i.e., the channel chart, such that the spatial geometry of actual UE locations is preserved in the chart. To achieve this goal, we first transform each \mathbf{H}_i into a $N_b \times L$ matrix $\mathbf{\Lambda}_i$, called signature map, with $L \ll N$, as shown in Fig.1. Then we use this signature map to perform a further dimensionality reduction (DR) to obtain the final chart $\mathbf{o}_i \in \mathbb{R}^2$ or \mathbb{R}^3 . Although this further DR can be accomplished by many approaches, such as Isomap [13], t-distributed stochastic neighbor embedding (t-SNE) or Laplacian eigenmap, these approaches cannot be easily used to predict on unseen data. Therefore, the SPCA and SSN are proposed for the DR from the signature map to the chart. The details of the proposed method are given below.

A. Signature map generation

To obtain the signature map, one needs firstly to construct a path from the raw discrete sequence. A path, constructed simply by linear interpolating the CIR sequence, usually doesn't suit the purpose of CC well. Therefore, we propose the cumulative sum of energy (CSE) path with time and basepoint augmentations. The detailed steps are given below.

²The proposed method, however, can be applied to multi-antenna scenarios, in which N_b denotes the number of antennas from all BSs. Alternatively, one can construct a path in the angular domain and generate a corresponding signature map, in particular when the spatial dimensionality is predominant.

³We use the tap to denote the more commonly known terminology of multipath-component. Although that each CIR is assumed to have the same length, the proposed approach can be applied directly to a dataset that has variable-length CIRs.

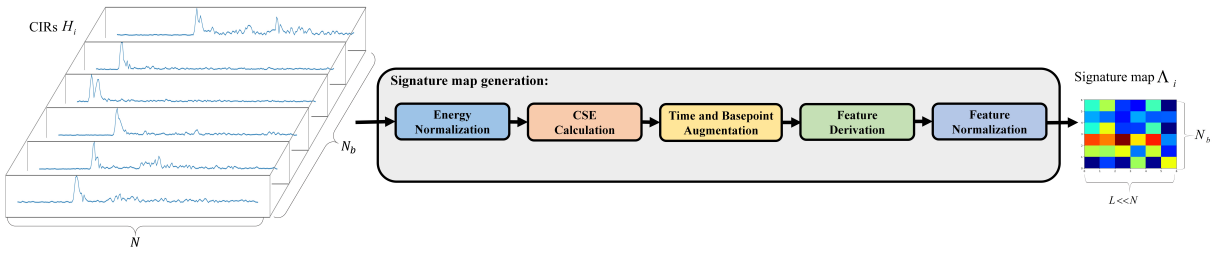


Fig. 1: An illustration of the signature map generation.

- **Energy normalization.** The first step is to normalize the total energy of CIR, which can solve the scaling problem owing to the large-scale fading. The resulting CIR can be written as an ordered sequence,

$$\{\mathbf{h}_n\}_{n=1}^N = ((a_1, b_1), (a_2, b_2), \dots, (a_N, b_N)) \quad (6)$$

where \mathbf{h}_n is a 2-tuple vector with $a_n, b_n \in \mathbb{R}$ representing the real and imaginary parts of the n -th tap, satisfying $\sum_{n=1}^N a_n^2 + b_n^2 = 1$.

- **Calculation of CSE sequence.** The second step is to obtain the CSE sequence, which is given by

$$\{c_n\}_{n=1}^N = (c_1, c_2, \dots, c_N) \quad (7)$$

where $c_n = \sum_{k=1}^n p_k$ and $p_k = a_k^2 + b_k^2$. Note that $c_N = 1$ after energy normalization of CIR. The CSE sequence is non-decreasing, which makes the mapping from the CSE path to signature become injective and the resulting features of signature have meaningful interpretations from geometrical or physical viewpoint.

- **Time augmentation.** The time augmentation intends to lift the sequence dimensionality and emphasize the time information, since the time information is crucial for CC in case of SISO scenarios. The operation for time augmentation is simply adding the timing information for each tap, i.e.,

$$\{\mathbf{c}_n^{(aug)}\}_{n=1}^N = ((c_1, t_1), (c_2, t_2), \dots, (c_N, t_N)) \quad (8)$$

where t_n is the time for the n -th tap. For CIRs measured with uniform sampling, $\{t_n\}_{n=1}^N$ is an evenly spaced sequence and depends on the sampling rate. If all samples in the dataset use the same sampling rate and have the same number of CIR lengths, $\{t_n\}_{n=1}^N$ can be set as $\{n/N\}_{n=1}^N$, in virtue of the signature property of invariance to reparameterization.

- **Basepoint augmentation.** The operation for basepoint augmentation is simply adding a 2-tuple zero vector at the start, i.e.,

$$\{\mathbf{c}_n^{(base)}\}_{n=0}^N = ((c_0, t_0), (c_1, t_1), (c_2, t_2), \dots, (c_N, t_N)) \quad (9)$$

Here $c_0 \triangleq 0$ and $t_0 \triangleq 0$. The purpose of basepoint augmentation is to make an alignment for the starting point of each time-augmented CSE sequence. By aligning the basepoint, the integrity of time and energy information is preserved, especially for CIRs with the first tap having the

highest energy. Because some signature features depend on the difference between the endpoint and starting point of the CSE sequence, the possibly important information of the first tap of CIRs will be lost if there is no basepoint augmentation.

- **Feature derivation.** With the time and basepoint augmented CSE sequence, a two-dimensional CSE path $X : [t_0, t_N] \rightarrow \mathbb{R}^2$ can be constructed by linear interpolation, which is given by

$$X(t) = \begin{cases} X_1(t) = c(t) \\ X_2(t) = t \end{cases} \quad (10)$$

where $c(t) = \frac{c_n - c_{n-1}}{t_n - t_{n-1}}(t - t_{n-1}) + c_{n-1}$ (for $t_{n-1} \leq t \leq t_n$) is a piece-wise linear function of time. Then its truncated signature can be obtained by (2) and (5). A practical implementation for calculating the signature can be found in [14]. We denote the obtained signature as a vector $\boldsymbol{\lambda} \in \mathbb{R}^L$, where L denotes the number of features and depends on the level at which the truncation is performed. Note that the complexity of calculating the signature is linear with respect to N , which usually does not bring much computational cost, given the significant complexity reduction on the subsequent procedures.

- **Feature normalization.** The obtained signature is further normalized across the dataset so that each feature is zero-mean and unit-variance.⁴

By performing the above operations for each CIR from each BS, the raw channel information of each sample \mathbf{H}_i is transformed into a more compact signature map Λ_i , which is used as the feature map for the subsequent CC.

B. SPCA and SSN

After obtaining the signature map, the inner product of the signature becomes a faithful similarity measure, and CC by PCA becomes attractive because of its practical implementation, computational efficiency, and the ability to inference on unseen data. The SPCA can also be viewed as a kernelized PCA. Moreover, we can further select a subset of vectors from the signature map, by which the computational complexity can be further reduced without degrading the CC performance seriously, as will be shown in Section IV.

⁴Note that, in addition to improving the training efficiency, this step can also reduce the homoskedastic-noise effect from noisy CI. In case of datasets with heteroskedastic noise, path averaging or signature averaging across consecutive CI can be used for denoising, and other advanced methods, such as [12], work as well.

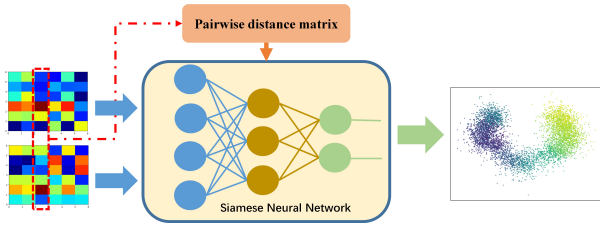


Fig. 2: An illustration of SSN based CC.

With the obtained signature map, Siamese network can be used to learn the chart, as shown in Fig.2. To train the network, We propose the following distance metric for any pair of signature maps,

$$\rho(\mathbf{\Lambda}_i, \mathbf{\Lambda}_j) \triangleq \|\mathbf{s}_i - \mathbf{s}_j\|_1 \quad (11)$$

where $\mathbf{s}_i = [s_1^{(i)}, s_2^{(i)}, \dots, s_m^{(i)}, \dots, s_{N_b}^{(i)}]^T \in \mathbb{R}^{N_b}$, $\|\cdot\|_1$ denotes the l^1 norm, and $s_m^{(i)}$ denotes one of the signature feature from the i -th sample and m -th BS, which is given by

$$s_m^{(i)} = \frac{1}{12} \sum_{n=1}^N p_n (t_N^2 + 2t_n^2 + 2t_{n-1}^2 + 2t_n t_{n-1} - 3t_N (t_n + t_{n-1})) \quad (12)$$

Note that we have removed the superscript (i) and subscript

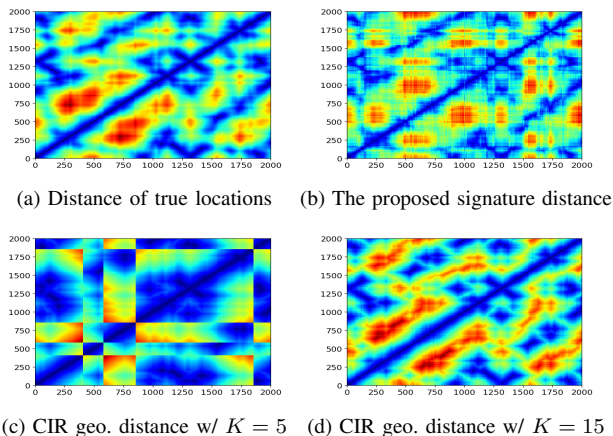


Fig. 3: Heatmaps for pairwise distance matrices.

m for each term of p_n and t_n for brevity. Unlike the CIR geodesic distance proposed in [2], the proposed signature distance can be a faithful metric for both local and global dissimilarity without constructing any neighborhood graph. Fig.3 shows some results about the heatmaps for the pairwise distance matrices of true radio environment, the proposed signature distance, and CIR geodesic distance with different neighborhood numbers, using the first 2K samples from the ultra wideband (UWB) dataset in [2]. As can be seen, the heatmap of the pairwise signature distance shows similar pattern with that of physical distance. Whereas the result of the CIR geodesic distance can be seriously degraded when the neighborhood number K is set inappropriately. With the distance metric for signature maps, the following loss function is proposed to train the Siamese network,

$$\mathcal{L}(\mathbf{o}_i, \mathbf{o}_j) = \sqrt{\sum_{(i,j) \in \mathcal{P}_{batch}} (\rho(\mathbf{\Lambda}_i, \mathbf{\Lambda}_j) - \|\mathbf{o}_i - \mathbf{o}_j\|_2)^2} \quad (13)$$

where $\mathcal{P}_{batch} := \{(i, j) | (i, j) \in \mathcal{D} \times \mathcal{D}\}$ is a set of index pairs with the cardinality being the batch number $|\mathcal{P}_{batch}| = N_{batch}$ and \mathbf{o}_i denotes the low-dimensional embedding for the i -th sample. Note that we intentionally remove a scaling factor in the loss function, which is usually proportional to the batch number. Instead, we normalize the pairwise distance matrix, which can speed up the training time and shows better results.

TABLE I: Simulation assumptions for InF-DH

Parameter	Value
Scenario	InF-DH
Hall size	120 × 60 m
Carrier frequency	3.5GHz
Bandwidth	100MHz
UE height	1.5m
Clutter parameters	density: 60%, height: 6m, size: 2m
Antenna configurations	1 element at BS and 1 element at UE,
Dimensionality of CIRs	18 × 256 × 2
Size of the dataset	6K for training and 2K for testing

TABLE II: Network architectures for the proposed SSNs

Layer Type	Output dimension		Kernel size
	InF-DH	5G/UWB	InF-DH/5G/UWB
Conv	16 × 18 × 6	16 × 6 × 6	3 × 3
Conv	32 × 18 × 6	32 × 6 × 6	5 × 5
Pooling	1 × 18 × 6	1 × 6 × 6	-
Dense	10	10	-
Dense	2	2	-

TABLE III: FLOPs comparison for different model input

Input Type	Dataset		
	InF-DH	5G	UWB
CIR magnitude	60.53M	3.86M	15.76M
Signature map (Ours)	1.42M	0.47M	0.47M

IV. EXPERIMENTAL RESULTS

The proposed method is evaluated in one synthetic dataset in the scenario of indoor factory with dense clutter and high base station (InF-DH) from the 3rd Generation Partnership Project (3GPP) [10] and two open-source real-filed datasets for 5G and ultra-wideband (UWB) systems [15]. The simulation assumptions for the InF-DH dataset are given in Table I. The configurations of 5G and UWB datasets can be found in [15]. We use the preprocessed samples for UWB and 5G datasets [2], in which the time of arrival (TOA) or the time difference of arrival (TDOA) information is embedded into the CIR. For all datasets, every sample is transformed to a $N_b \times L$ signature map with $N_b = 18$ for InF-DH, $N_b = 6$ for 5G and UWB datasets, and $L = 6$ representing the number of signature features from the 2nd to the 4th level. The first level signature features (which are c_N and t_N) are discarded since they are uninformative after normalizing the CIR energy. Compared with the dimensionality of CIRs, the feature number has been reduced more than 87% for 5G and 97% for InF-DH and UWB datasets, which means a significant reduction in complexity for subsequent procedures of CC.

The performance of local similarity for CC is evaluated in terms of the continuity (CT) and trustworthiness (TW) [1]. The value of these two metrics ranges from 0 to 1, and neighbor

TABLE IV: Experimental results for InF-DH dataset

Method	Training dataset				Testing dataset			
	CT \uparrow	TW \uparrow	MAE \downarrow	CE90 \downarrow	CT \uparrow	TW \uparrow	MAE \downarrow	CE90 \downarrow
SPCA (Ours)	0.918	0.892	14.73 \pm 0.16 (m)	25.97 \pm 0.32 (m)	0.914	0.892	14.67 \pm 0.16 (m)	25.58 \pm 0.33 (m)
CIR PCA	0.949	0.961	17.04 \pm 0.6 (m)	31.95 \pm 0.5 (m)	0.946	0.960	17.04 \pm 0.6 (m)	31.95 \pm 0.5 (m)
FSSN (Ours)	0.935	0.921	13.78 \pm 0.16 (m)	24.55 \pm 0.29 (m)	0.931	0.920	13.54 \pm 0.15 (m)	23.88 \pm 0.33 (m)
PSSN (Ours)	0.960	0.957	12.43 \pm 0.16 (m)	23.11 \pm 0.33 (m)	0.957	0.956	12.44 \pm 0.15 (m)	22.67 \pm 0.34 (m)
CIR Sia.	0.941	0.935	18.92 \pm 0.22 (m)	33.3 \pm 0.57 (m)	0.941	0.938	19.08 \pm 0.22 (m)	33.38 \pm 0.65 (m)

TABLE V: Experimental results for 5G dataset

Method	Training dataset				Testing dataset			
	CT \uparrow	TW \uparrow	MAE \downarrow	CE90 \downarrow	CT \uparrow	TW \uparrow	MAE \downarrow	CE90 \downarrow
SPCA (Ours)	0.906	0.839	2.00 \pm 0.10 (m)	3.63 \pm 0.21 (m)	0.908	0.845	1.93 \pm 0.09 (m)	3.54 \pm 0.21 (m)
CIR PCA	0.911	0.855	4.25 \pm 0.07 (m)	7.66 \pm 0.17 (m)	0.914	0.864	4.11 \pm 0.05 (m)	7.37 \pm 0.13 (m)
FSSN (Ours)	0.915	0.843	4.59 \pm 0.04 (m)	7.74 \pm 0.17 (m)	0.919	0.855	4.27 \pm 0.04 (m)	7.61 \pm 0.18 (m)
PSSN (Ours)	0.987	0.986	1.30 \pm 0.02 (m)	2.24 \pm 0.03 (m)	0.984	0.983	1.34 \pm 0.02 (m)	2.40 \pm 0.03 (m)
CIR Sia.	0.980	0.979	1.54 \pm 0.02 (m)	2.74 \pm 0.04 (m)	0.976	0.974	1.60 \pm 0.02 (m)	2.93 \pm 0.04 (m)
CIR Sia. in [2]	0.986	0.986	1.40 (m)	2.35 (m)	0.983	0.982	1.46 (m)	2.48 (m)

TABLE VI: Experimental results for UWB dataset

Method	Training dataset				Testing dataset			
	CT \uparrow	TW \uparrow	MAE \downarrow	CE90 \downarrow	CT \uparrow	TW \uparrow	MAE \downarrow	CE90 \downarrow
SPCA (Ours)	0.976	0.962	1.52 \pm 0.02 (m)	2.75 \pm 0.04 (m)	0.976	0.965	1.46 \pm 0.02 (m)	2.72 \pm 0.04 (m)
CIR PCA	0.934	0.825	3.79 \pm 0.07 (m)	7.49 \pm 0.22 (m)	0.941	0.874	3.51 \pm 0.05 (m)	6.33 \pm 0.14 (m)
FSSN (Ours)	0.980	0.970	1.33 \pm 0.01 (m)	2.35 \pm 0.02 (m)	0.978	0.970	1.33 \pm 0.01 (m)	2.38 \pm 0.03 (m)
PSSN (Ours)	0.997	0.996	0.66 \pm 0.01 (m)	1.24 \pm 0.02 (m)	0.996	0.996	0.67 \pm 0.01 (m)	1.24 \pm 0.02 (m)
CIR Sia.	0.992	0.991	0.88 \pm 0.01 (m)	1.60 \pm 0.03 (m)	0.991	0.990	0.87 \pm 0.01 (m)	1.58 \pm 0.02 (m)
CIR Sia. in [2]	0.997	0.997	0.69 (m)	1.30 (m)	0.997	0.996	0.72 (m)	1.28 (m)

points that are embedded far away from each other decrease CT, whereas far away points that are embedded as neighbor points decrease TW. For measuring global dissimilarity, we perform an affine transformation from the chart to real coordinates and evaluate the mean absolute errors (MAE) and the 90th-percentile of the cumulative distribution function of the error (CE90) in units of meters. We randomly choose 100 labeled samples to obtain the least-squares estimation of the affine matrix and perform 1K experiments to obtain the mean and standard deviation of MAE and CE90. Moreover, the proposed SPCA and SSN are compared with CIR based methods including CIR magnitude based PCA or Siamese network [2]. For SSN based CC, we further evaluate two approaches, namely the full SSN (FSSN) and partial SSN (PSSN) based charting. FSSN uses the signature map as network input and also uses it to produce the pairwise distance matrix by (11), and the PSSN only uses the signature map as network input and the pairwise distance matrix is generated by calculating CIR geodesic distance. Moreover, the Adam optimizer is used for training all networks with 50 epochs, and the batch size is set to be 50 for InF-DH and 500 for both 5G and UWB datasets, and the learning rate is set to be 1e-4 for InF-DH and 1e-3 for both 5G and UWB datasets.

The network architectures and output dimensions for each layer are given in Table II. The model consists of two Conv layers, one adaptive average pooling, and two dense layers. Each Conv layer consists of a 2-D convolutional layer, a batch normalization (BN) and a rectified linear unit (ReLU) as the activation function. The number of floating-point operations

(FLOPs) for the network with CIRs or the signature map as model input are given in Table III. It can be seen that the number of FLOPs is reduced significantly for all datasets.

A. Results for InF-DH dataset

The true UE locations and the charting results after affine transformation are given in Fig.4, and detailed results for all evaluated methods are given in Table IV. For PCA based CC, we select the vector \mathbf{s}_i from the signature map for each sample to do PCA, which means we only need to do SVD for an 18×18 covariance matrix rather than a 4608×4608 matrix for CIR based PCA. Moreover, SPCA shows better results on global performance in terms of MAE and CE90 and slightly degraded local similarity in terms of CT and TW, compared with CIR based PCA. For Siamese network based CC, both FSSN and PSSN show better results on global performance and similar results on local similarity in comparison of CIR based method. It thus implies that better performance and significant complexity reduction can be achieved simultaneously with our proposed method.

B. Results for 5G and UWB datasets

For the 5G dataset, the experimental results are given in Table V and Fig.5. For PCA based method, the vectorized signature map is used to obtain the covariance matrix and more components are used for the affine transformation. It can be seen that SPCA shows much better results on global similarity in terms of MAE and CE90 compared with CIR based PCA. For Siamese network based charting, the result reported in [2]

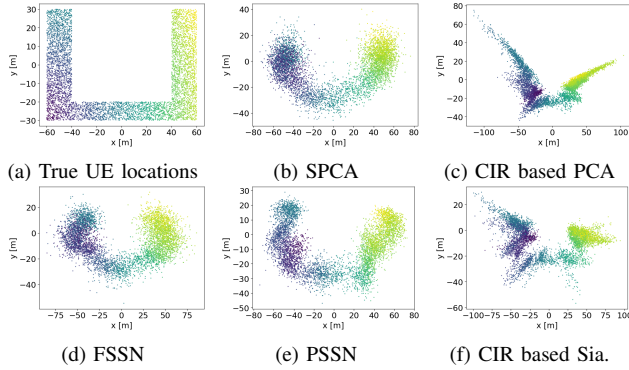


Fig. 4: Ground-truth UE locations and CC results after affine transformation for InF-DH dataset.

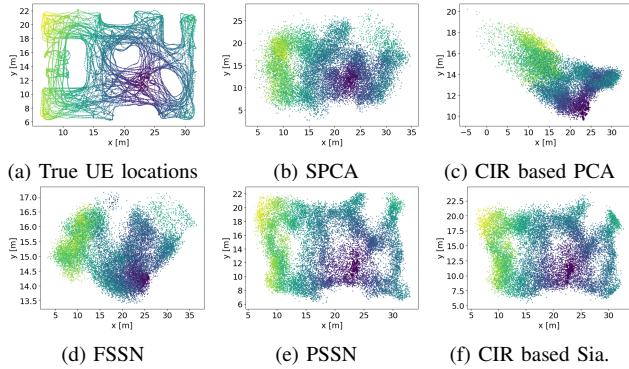


Fig. 5: Ground-truth UE locations and CC results after affine transformation for 5G dataset.

is also given, which is obtained by a more complex Siamese network and using all training samples to perform the affine transformation. It shows that PSSN achieves the best results for both local and global similarity among all methods, with a complexity reduction about 88% (as shown in Table III). Moreover, the results of FSSN are unexpectedly worse than PSSN and CIR based methods. The reason is that only TDOA information is embedded in the CIR and the reference BS for the measurement of TDOA is not even fixed, which decreases the reliability for the proposed signature distance metric.

For the UWB dataset, experimental results are given in Table VI and Fig. 6. For PCA based method, due to the TOA information is kept in each CIR, we select the vector s_i for constructing the covariance matrix just like the SPCA for InF-DH dataset, which can further reduce the complexity without sacrificing the performance. It can be seen that both the local and global performance are greatly improved when using SPCA instead of CIR based PCA, and the performance can be further improved by FSSN. Compared with the result from [2], PSSN achieves better global similarity and almost the same local similarity, with a complexity reduction more than 97%.

V. CONCLUSIONS

In this paper, a novel signature based approach for global CC is proposed, in which a compact signature map is extracted from CIRs and can be used for PCA or Siamese network

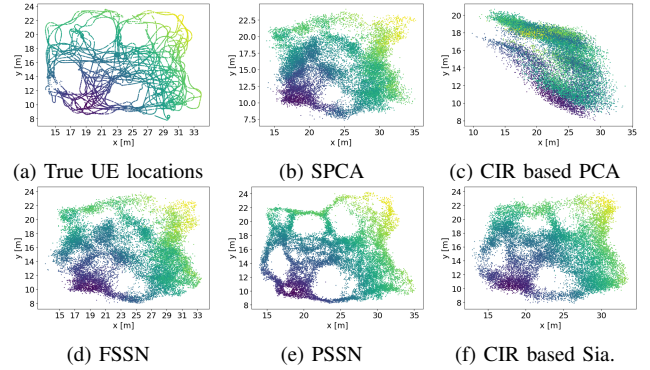


Fig. 6: Ground-truth UE locations and CC results after affine transformation for UWB dataset.

based CC. Moreover, a novel distance metric, which does not need to construct neighborhood graph, is proposed for training Siamese networks. The experimental results show that the proposed approach can achieve better performance on global and local similarity than CIR based methods, with significantly reduced complexity.

REFERENCES

- [1] C. Studer, S. Medjkouh, E. Gonultas, et al. "Channel charting: locating users within the radio environment using channel state information," IEEE Access, vol. 6, pp. 47 682–47 698, Aug. 2018.
- [2] M. Stahlke, G. Yammine, T. Feigl, et al. "Indoor localization with robust global channel charting: a time-distance-based approach," IEEE Transactions on Machine Learning in Communications and Networking, vol.1, pp. 3-17, Mar. 2023.
- [3] S. Taner, V. Palhares, and C. Studer, "Channel charting in real-world coordinates," In Proc. IEEE Globe Communications Conference (GlobeCom), Dec. 2023, pp. 3940-3946.
- [4] J. Zhang, F. Wu, Y. Yang, J. Chen, "Beam tracking: a channel charting and neighborhood search based method," In Proc. IEEE Globe Communications Conference (GlobeCom), Dec. 2023, pp. 807-812.
- [5] L. Ribeiro, M. Leinoneal, I. Rathnayaka, et al. "Channel charting aided pilot allocation in multi-cell massive MIMO mMTC networks," IEEE 23rd International Workshop on Signal Processing Advances in Wireless Communication (SPAWC), July 2022.
- [6] K. T. Chen, "Integration of paths, geometric invariants and a generalized Baker-Hausdorff formula." Annals of Mathematics, vol.65, no.1, pp.163-178, Jan. 1957.
- [7] T. J. Lyons, M. Caruana, T. Lévy, Differential Equations Driven by Rough Paths, Springer, Berlin, 2007.
- [8] F. J. Király, H. Oberhauser, "Kernels for Sequentially Ordered Data" Journal of Machine Learning Research, vol.20, pp.1-45, 2019.
- [9] T. J. Lyons, H. Ni, and H. Oberhauser, "A feature set for streams and an application to high-frequency financial tick data," International Conference on Big Data Science and Computing (ICBDC), Aug. 2014.
- [10] 3GPP TR.38.901 V16.1.0, "Study on channel model for frequencies from 0.5 to 100GHz (Rel-16)," 2019.
- [11] P. Ferrand, A. Decurninge, L. G. Ordoñez, and M. Guillaud, "Triplet-based wireless channel charting: architecture and experiments," IEEE J. Sel. Areas Commun., vol. 39, no. 8, pp. 2361–2373, Aug. 2021.
- [12] L. Zhao, Q. Xiong, and et al., "Enabling Accurate Positioning in NLOS Scenarios by Hybrid Machine Learning with Denoising and Inpainting," IEEE Vehicular Technology Conference (VTC2022-Fall), Sep. 2022.
- [13] J. B. Tenenbaum, V. Silva, and J. C. Langford, "A global geometric framework for nonlinear dimensionality reduction," Science, vol.290, no.5500, pp. 2319-2323, Dec. 2002.
- [14] J. F. Reizenstein and B. Graham, "Algorithm 1004: the iisignature library: efficient calculation of iterated-integral signatures and log signatures." ACM Trans. Math. Softw. vol.46, no.1, March 2020.
- [15] Fraunhofer IIS, Fingerprinting dataset for positioning. Available: <https://www.iis.fraunhofer.de/en/ff/1v/dataanalytics/pos/fingerprinting-dataset-for-positioning.html>